

Discontinuous Transitions Towards Vortex Condensates in Buoyancy-Driven Rotating Turbulence: Analogies with First-Order Phase Transitions

Xander M. de Wit, Andrés J. Aguirre Guzmán, Herman J.H. Clercx, and Rudie P.J. Kunnen*
*Fluids and Flows group, Department of Applied Physics and J. M. Burgers Centre for Fluid Dynamics,
Eindhoven University of Technology, P.O. Box 513, 5600 MB Eindhoven, Netherlands*
(Dated: May 16, 2022)

Employing immediate analogies with phase transitions in equilibrium statistical mechanics, we explore the transitions between turbulent states from a 3D flow state towards a quasi-2D condensate known as the large-scale vortex (LSV). Using direct numerical simulations of rotating Rayleigh-Bénard convection, we vary the Rayleigh number Ra as control parameter and study the system response (strength of the LSV) in terms of order parameters assessing the energetic content in the flow and the upscale energy flux. By sensitively probing the boundaries of the domain of existence of the LSV, we find discontinuous transitions and we identify the presence of a hysteresis loop as well as nucleation & growth type of dynamics, manifesting the striking correspondence with first-order phase transitions in equilibrium statistical mechanics. We show furthermore that the creation of the condensate state coincides with a discontinuous transition of the energy transport into the largest mode of the system.

DOI: xxx

A hallmark feature of 3D turbulence is the forward energy cascade, transporting kinetic energy from large scales to ever smaller scales as described by the celebrated theory of Kolmogorov [1]. In many geophysical and astrophysical flows, however, velocity fluctuations are largely suppressed in one direction as a consequence of, for example, confinement [2–4], strong magnetic fields [5, 6] or fast rotation [7–10], rendering the flow quasi-2D. This leads to the development of an inverse energy flux, akin to fully 2D turbulence [11, 12], transporting energy from smaller to larger scales. Ultimately, this can lead to accumulation of kinetic energy at the largest available scales, followed by condensation into a vertically coherent large-scale vortex (LSV) structure at the domain size [13]. These LSVs are believed to play a crucial role in for example the formation of the Earth’s magnetic field [14–16].

We approach the transition from a 3D forward cascading state to the condensate state from the viewpoint of statistical mechanics, considering the behavior of an order parameter that measures the strength of the LSV as a function of a control parameter of the flow throughout this transition. Although turbulent flow systems are inherently out-of-equilibrium due to the dissipative character of turbulence itself, it has been surmised that these condensate states may be in close resemblance with statistical-physical thermal equilibrium states, though this remains conjectural [13, 17]. Moreover, classifying the transitions to condensate states from a framework of phase transitions in equilibrium statistical mechanics has shown to be an insightful approach in various other rotating flow systems [8, 18, 19].

These earlier works, however, have focused on more artificial, idealized flow models where the turbulent forcing occurs at a single well-defined length scale. Here, we characterize for the first time the LSV transition in

a natural, broadband-forced system of rotating convection, which is ubiquitous in geophysical and astrophysical flows. The natural buoyant forcing over a broad range of scales obfuscates the strict separation of the injection, dissipation and condensation scale. Although one can expect that in such natural turbulent systems, any transitions between different states are washed out and become gradual, we find that the transition towards the condensate state is in fact sharp and discontinuous and we show the remarkable analogy with first-order phase transitions.

We consider the canonical system of rotating Rayleigh-Bénard convection, in which the flow is driven by buoyancy through a temperature difference ΔT between the bottom and top of the domain, while being simultaneously affected by strong background rotation Ω along the vertical axis. The input space to this problem is described by three dimensionless numbers: the Rayleigh number $Ra = g\alpha\Delta TH^3/(\nu\kappa)$, quantifying the strength of the thermal forcing, the Ekman number $Ek = \nu/(2\Omega H^2)$, representing the (inverse) strength of rotation and the Prandtl number $Pr = \nu/\kappa$, containing the diffusive properties of the fluid. Here, g denotes gravitational acceleration, H is the domain height and α , ν and κ represent the thermal expansion coefficient, kinematic viscosity and thermal diffusivity of the fluid, respectively. The system is non-dimensionalized into convective units using H , ΔT and the free-fall velocity $U = \sqrt{g\alpha\Delta TH}$.

We solve the full governing set of Boussinesq Navier-Stokes equations through direct numerical simulation (DNS), employing the finite-difference code described in Refs. [20, 21] on a Cartesian grid with periodic side-walls and stress-free boundary conditions at the top and bottom. For the width D of the domain, we choose $D/H = 10\mathcal{L}_c$ with $\mathcal{L}_c = 4.8Ek^{1/3}$ the most unstable wavelength at onset of convection [22]. We use reso-

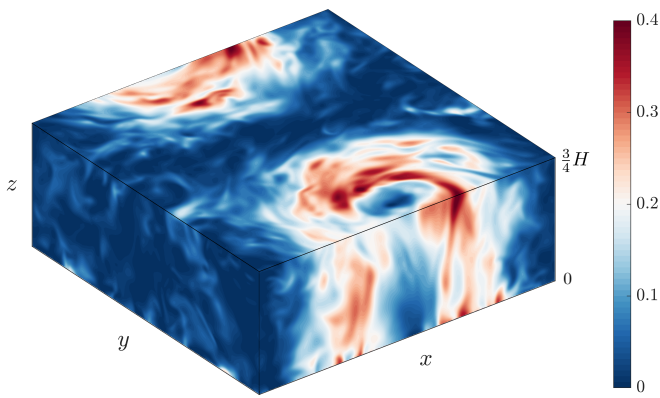


FIG. 1. Snapshot of horizontal kinetic energy (in units of U^2) of the LSV-forming case $Ra = 1.7 \times 10^7$, truncated at three-quarter height to reveal a cross section of the LSV.

lutions of $256 \times 256 \times (128-144)$, ensuring at least 10 grid cells within the thermal boundary layers and we resolve down to less than two times the Kolmogorov length, which is well within the limits established in Ref. [23].

For numerical convenience, we use $Pr = 1$ and $Ek = 10^{-4}$, for which stable LSVs have been observed in earlier DNSs over a limited range of Ra [24–26]. Upon increasing Ra from the onset of convection, the two boundaries of the domain of existence of the LSV are crossed. At the low- Ra transition, the LSV develops as sufficient turbulent forcing is obtained to set-up the upscale transport into the condensate, whereas at the high- Ra transition, the LSV breaks down as too strong thermal forcing renders the flow insufficiently rotationally constrained, breaking the quasi-2D conditions for upscale energy flux [24, 25]. We carry out a total of 46 runs at varying Ra , concentrated around both LSV transitions.

In order to analyze the LSV, we decompose the flow field $\mathbf{u} = u\mathbf{e}_x + v\mathbf{e}_y + w\mathbf{e}_z$ into a 2D (vertically averaged) barotropic flow and a 3D (depth-dependent) baroclinic flow, i.e. $\mathbf{u} = \mathbf{u}^{2D} + \mathbf{u}^{3D}$, where [24, 26–30]

$$\mathbf{u}^{2D} = \bar{u}\mathbf{e}_x + \bar{v}\mathbf{e}_y, \quad \mathbf{u}^{3D} = \underbrace{(u - \bar{u})}_{u'}\mathbf{e}_x + \underbrace{(v - \bar{v})}_{v'}\mathbf{e}_y + w\mathbf{e}_z, \quad (1)$$

where the overbar $\bar{\dots}$ denotes vertical averaging. Since the LSV is a largely vertically coherent structure (see Fig. 1), it resides primarily in the 2D field, whereas the turbulent baroclinic fluctuations are captured by the 3D field. Accordingly, we decompose the total kinetic energy $E_{\text{tot}} = \frac{1}{2}\langle |\mathbf{u}|^2 \rangle$ into 2D and (horizontal and vertical) 3D contributions $E_{\text{tot}} = E^{2D} + E_H^{3D} + E_V^{3D}$ as

$$E^{2D} = \frac{1}{2}\langle \bar{u}^2 + \bar{v}^2 \rangle, \quad E_H^{3D} = \frac{1}{2}\langle u'^2 + v'^2 \rangle, \quad E_V^{3D} = \frac{1}{2}\langle w^2 \rangle, \quad (2)$$

where angular brackets $\langle \dots \rangle$ represent an average over the full spatial domain. We also consider the energy spec-

trum of the 2D flow from its Fourier transform $\hat{\mathbf{u}}_{k_x k_y}^{2D}$ as

$$\hat{E}^{2D}(K) = \sum_{K \leq \sqrt{k_x^2 + k_y^2} < K+1} \frac{1}{2} |\hat{\mathbf{u}}_{k_x k_y}^{2D}|^2, \quad (3)$$

where we normalize the wavenumber K by the box-size mode $2\pi/D$, such that the LSV occupies the $K = 1$ mode of the spectrum.

In Fig. 2, the different components of kinetic energy are provided over the range of considered Ra , crossing both LSV transitions. From the (largest mode of) 2D energy that captures the LSV, we find a substantial discontinuity at both boundaries of the LSV state. At the high- Ra transition, we find that this transition is hysteretic: the morphology of the flow depends on its history and/or initial conditions. These findings are in line with Ref. [26], showing this bistability of an LSV and a non-LSV state for one case in this parameter range. For decreasing Ra from a non-LSV state, the lower branch of the hysteresis loop is followed (open diamonds), while for increasing Ra from an LSV state, the flow adheres to the upper hysteretic branch (filled squares), see Fig. 2. Note the remarkably large discontinuity in the lower hysteretic branch, where the flow transitions directly from a non-LSV state into nearly the strongest LSV forming state. Hysteretic transitions are rare in fluid turbulence, being observed, e.g., in the transition between different turbulent states of Taylor-Couette flow [31] and for the LSV transition in a rotating flow system with a *sharp bandwidth* Taylor-Green forcing [19].

At the low- Ra transition, on the other hand, we observe no hysteresis. Considering the cases directly above

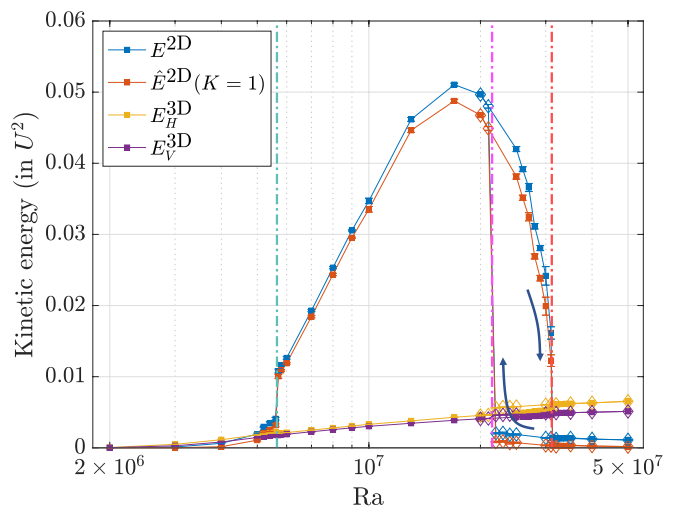


FIG. 2. Averaged kinetic energy components as a function of Ra . Filled squares: upper hysteretic branch of the high- Ra transition; open diamonds: lower hysteretic branch. The cyan dashed-dotted line denotes the low- Ra LSV transition, while the magenta and red lines denote the LSV transition of the lower and upper branch of the high- Ra transition, respectively.

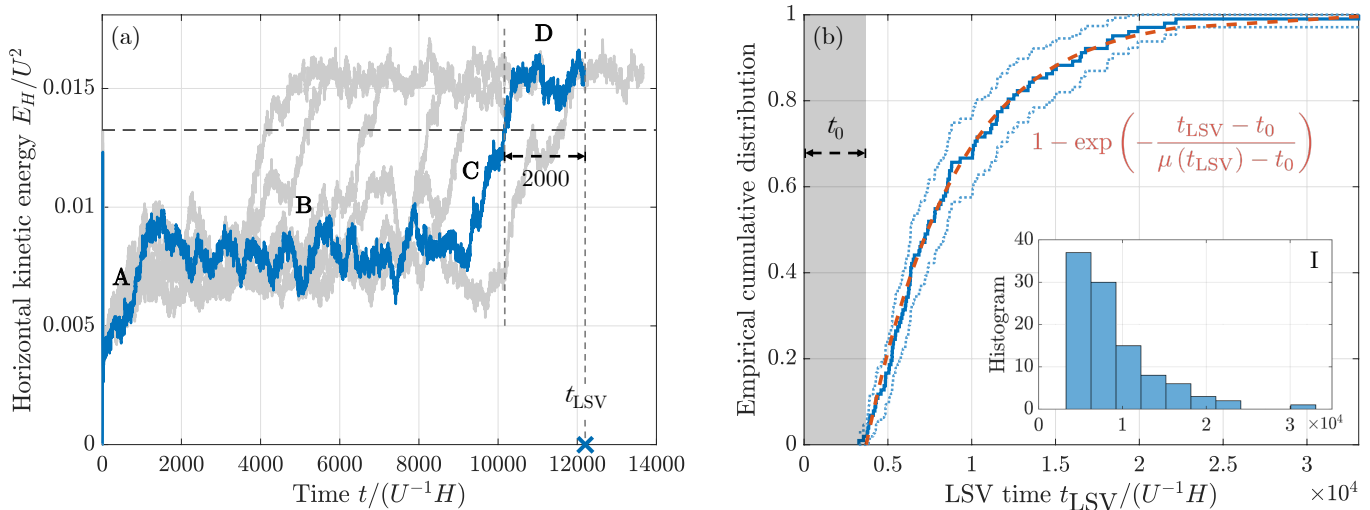


FIG. 3. Panel (a): time evolution of horizontal kinetic energy of seven of the runs in the ensemble of the LSV-forming case $Ra = 6 \times 10^6$ close to the transition. We distinguish four stages: an initialization phase (A), a metastable underdeveloped plateau state showing alternating jets (B), (quick) growth of the LSV (C) and the stably developed LSV state (D). The horizontal dashed line denotes the threshold to be crossed and sustained for 2000 convective time units ($U^{-1}H$) before the LSV is said to be completely developed, which defines the time point t_{LSV} , depicted by the blue cross. Panel (b): cumulative distribution of t_{LSV} of the ensemble (blue solid line) with 95% confidence bounds (blue dotted lines). It is fitted by an exponential distribution (red dashed line) as provided by Eq. (4) and in the figure. Inset (I) shows the histogram corresponding to the same distribution.

the LSV transition, however, we find that the growth of the LSV from a non-LSV state is non-monotonic: the flow shows an evident plateau during which the LSV has not yet developed, before finally growing into the stable LSV state, see Fig. 3a. The flow in this plateau state shows morphological similarities with the jet state observed in rectangular domains [32, 33], but alternates between being predominantly in the x - and y -direction. We hypothesize that the growth behavior found here signifies a nucleation & growth type of dynamics that is observed in plentiful different systems throughout physics [34–37]. To substantiate this conjecture, we simulate an ensemble of 100 additional runs at $Ra = 6 \times 10^6$ with statistically perturbed initial conditions, using a reduced resolution of $128 \times 128 \times 72$ for computational feasibility. Classical nucleation theory [38–40] then predicts an exponential distribution of the waiting time spent in the metastable plateau state (stage B in Fig. 3a).

To investigate this distribution, we define a time point t_{LSV} at which the LSV is said to have stably developed once a threshold of horizontal kinetic energy is surpassed and sustained for 2000 convective time units, see Fig. 3a. The obtained empirical cumulative distribution is then fitted with an exponential distribution

$$CDF(t_{\text{LSV}}) = 1 - \exp\left(-\frac{t_{\text{LSV}} - t_0}{\underbrace{\mu(t_{\text{LSV}}) - t_0}_{\tau_w}}\right), \quad (4)$$

where the fit parameter t_0 can be interpreted as the (fixed) contributions of the initialization, growth and stable LSV stages (A, C and D in Fig. 3a). Here, $\mu(t_{\text{LSV}})$

denotes the mean of t_{LSV} , providing the maximum-likelihood estimate for the typical waiting time τ_w in this distribution. Fig. 3b shows that there is excellent agreement between the hypothesized and the obtained distribution: the exponential distribution remains everywhere in between the 95% confidence bounds of the empirical distribution. Signs of exponentiality of waiting times have been observed in the LSV-forming system of *artificially* forced thin-layer turbulence [41]. Our findings suggest that, indeed, the turbulent fluctuations must somehow randomly ‘nucleate’ the LSV in order to commence its growth.

We can interpret these findings from the perspective of equilibrium statistical mechanics. The non-LSV state and the LSV state can then be understood as two distinct minima, separated by a barrier in the ‘free energy’, or perhaps here more appropriately, a barrier of reduced flow stability. Near the low- Ra transition, this barrier is surmountable through the turbulent fluctuations, leading to the characteristic nucleation & growth type of dynamics as predicted by classical nucleation theory, whereas at the high- Ra transition, the barrier becomes insurmountable within any physically realizable timescale, resulting in hysteresis. This shows, from the perspective of equilibrium statistical mechanics, the pertinent analogy of these sharp flow transitions with first-order phase transitions [42].

To understand how the LSV is energetically sustained, we compute the shell-to-shell kinetic energy transfer [43–48], distinguishing the 3D to 2D (baroclinic to

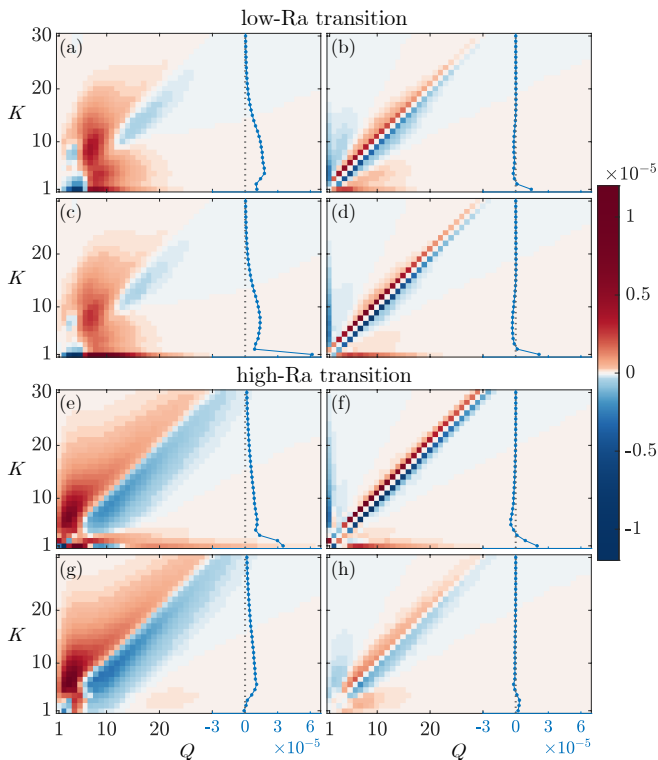


FIG. 4. Time-averaged kinetic energy transport from 3D (left panels) or 2D (right panels) modes Q to 2D modes K , i.e. $T_{3D}(K, Q)$ and $T_{2D}(K, Q)$, respectively, in units of $U^3 H^{-1}$. Blue lines denote $\mathcal{T}_{3D}(K)$ (left) and $\mathcal{T}_{2D}(K)$ (right). The low-Ra transition is crossed from (a,b) [$\text{Ra} = 5.6 \times 10^6$] to (c,d) [$\text{Ra} = 5.7 \times 10^6$], while the high-Ra transition of the upper hysteretic branch is crossed from (e,f) [$\text{Ra} = 3.10 \times 10^7$] to (g,h) [$\text{Ra} = 3.13 \times 10^7$].

barotropic) transport [27, 30]

$$T_{3D}(K, Q) = -\left\langle \mathbf{u}_K^{2D} \cdot \overline{(\mathbf{u}^{3D} \cdot \nabla \mathbf{u}_Q^{3D})} \right\rangle, \quad (5a)$$

and the 2D to 2D (barotropic to barotropic) transport

$$T_{2D}(K, Q) = -\left\langle \mathbf{u}_K^{2D} \cdot (\mathbf{u}^{2D} \cdot \nabla \mathbf{u}_Q^{2D}) \right\rangle, \quad (5b)$$

describing the energetic transport into the Fourier-filtered 2D flow field \mathbf{u}_K^{2D} of wavenumber K from 3D and 2D modes Q through triadic interactions arising from the advective term of Navier-Stokes. If $T_{3D}, T_{2D} > 0$, there is a net transfer of kinetic energy from mode Q to mode K and vice-versa. We also consider the transport into 3D mode K from the full (unfiltered) flow components $\mathcal{T}_{3D}(K) = \sum_Q T_{3D}(K, Q)$ and $\mathcal{T}_{2D}(K) = \sum_Q T_{2D}(K, Q)$, by summing over the donating modes Q .

The results for the shell-to-shell energy transfer throughout the LSV transitions are provided in Fig. 4. The two main energy fluxes are apparent in both T_{3D} and T_{2D} . Near the diagonal, one can observe the direct forward cascade, transporting energy from Q to slightly higher modes K . In the bottom row $K = 1$, the upscale

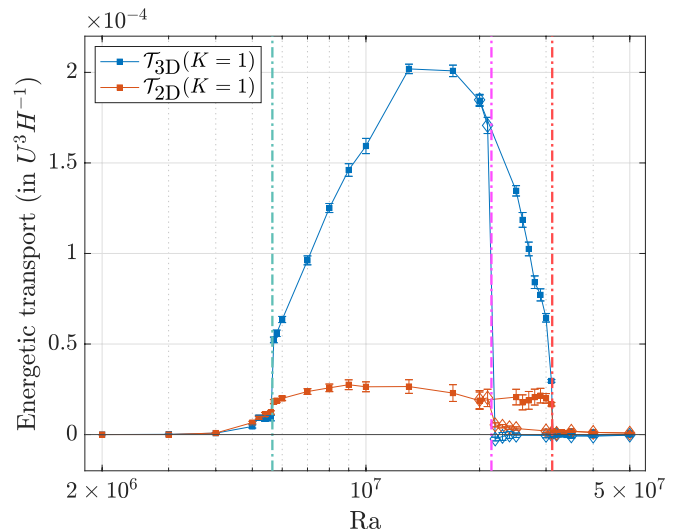


FIG. 5. Total 3D $\mathcal{T}_{3D}(K=1)$ (blue) and 2D $\mathcal{T}_{2D}(K=1)$ (red) transport of kinetic energy into the 2D $K=1$ mode averaged over time as a function of Ra . Symbols and vertical lines are as in Fig. 2.

energy flux into the LSV can be appreciated. This energy flux is non-local: energy is transported directly from virtually all scales in the system into the box scale of the LSV, without participation of intermediate scales.

Fig. 5 shows the energetic transport into the box-size mode as a function of Ra . It makes clear that also the upscale transport into the LSV exhibits a discontinuous transition. Furthermore, we can observe that the 3D transport is the dominant component in the forcing of the LSV.

We argue that this upscale transport provides a clue to understand the physical mechanism behind the nucleation & growth and hysteretic behavior. As detailed in Refs. [26, 30], the upscale transport contains a positive feedback loop, where the presence of the LSV itself enhances the upscale transport into the box-size mode. This seems intuitive, as the predominantly cyclonic LSV locally increases the total vorticity (background rotation + flow vorticity), thereby strengthening the quasi-2D conditions and hence the upscale transport. This mechanism allows the LSV to develop once it is ‘nucleated’ and lets the LSV remain stably self-sustained over the hysteresis loop.

In this Letter, we have shown a fluid turbulence transition in a natural broadband-forced system of rotating Rayleigh-Bénard convection, where the transition is sharply discontinuous, regardless of the lack of a clear separation of scales. We provide firm evidence of nucleation & growth and hysteresis in these transitions, exhibiting the profound correspondence with first-order phase transitions in equilibrium statistical mechanics. This motivates further theoretical investigations of the quasi-2D condensate transition based on statistical me-

chanics and illustrates how it can provide elucidating insights in understanding turbulent flow transitions, in spite of the deterministic-chaotic nature of turbulence itself. By demonstrating the underlying mechanisms by which the flow transitions to an LSV state, we advance the understanding of how these remarkable large-scale structures can emerge in various constrained turbulent flow systems in nature.

We thank W.G. Ellenbroek for careful reading of the manuscript. A.J.A.G. and R.P.J.K. received funding from the European Research Council (ERC) under the European Union's Horizon 2020 research and innovation programme (Grant Agreement No. 678634). We are grateful for the support of the Netherlands Organisation for Scientific Research (NWO) for the use of supercomputer facilities (Cartesius) under Grants No. 2019.005 and No. 2020.009.

* r.p.j.kunnen@tue.nl

- [1] A. N. Kolmogorov, Doklady Akademiia Nauk SSSR **32**, 19 (1941).
- [2] S. J. Benavides and A. Alexakis, J. Fluid Mech. **822**, 364 (2017).
- [3] S. Musacchio and G. Boffetta, Phys. Fluids **29**, 111106 (2017).
- [4] S. Musacchio and G. Boffetta, Phys. Rev. Fluids **4**, 022602 (2019).
- [5] A. Alexakis, Phys. Rev. E **84**, 056330 (2011).
- [6] K. Seshasayanan, S. J. Benavides, and A. Alexakis, Phys. Rev. E **90**, 051003 (2014).
- [7] L. M. Smith, J. R. Chasnov, and F. Waleffe, Phys. Rev. Lett. **77**, 2467 (1996).
- [8] K. Seshasayanan and A. Alexakis, J. Fluid Mech. **841**, 434 (2018).
- [9] T. Pestana and S. Hickel, Phys. Rev. E **99**, 053103 (2019).
- [10] A. van Kan and A. Alexakis, J. Fluid Mech. **899**, A33 (2020).
- [11] R. H. Kraichnan, Phys. Fluids **10**, 1417 (1967).
- [12] G. K. Batchelor, Phys. Fluids **12**, II (1969).
- [13] A. Alexakis and L. Biferale, Phys. Rep. **767-769**, 1 (2018).
- [14] J. M. Aurnou, M. A. Calkins, J. S. Cheng, K. Julien, E. M. King, D. Nieves, K. M. Soderlund, and S. Stellmach, Phys. Earth Planet. Inter. **246**, 52 (2015).
- [15] C. Guervilly, D. W. Hughes, and C. A. Jones, Phys. Rev. E **91**, 041001 (2015).
- [16] P. H. Roberts and E. M. King, Rep. Progr. Phys. **76**, 096801 (2013).
- [17] F. Bouchet and A. Venaille, Phys. Rep. **515**, 227 (2012).
- [18] A. Alexakis, J. Fluid Mech. **769**, 46 (2015).
- [19] N. Yokoyama and M. Takaoka, Phys. Rev. Fluids **2**, 092602 (2017).
- [20] R. Verzicco and P. Orlandi, J. Comput. Phys. **123**, 402 (1996).
- [21] R. Ostilla-Monico, Y. Yang, E. P. van der Poel, D. Lohse, and R. Verzicco, J. Comput. Phys. **301**, 308 (2015).
- [22] S. Chandrasekhar, *Hydrodynamic and Hydromagnetic Stability* (Oxford University Press, 1961).
- [23] R. Verzicco and R. Camussi, J. Fluid Mech. **477**, 19 (2003).
- [24] B. Favier, L. J. Silvers, and M. R. E. Proctor, Phys. Fluids **26**, 096605 (2014).
- [25] C. Guervilly, D. W. Hughes, and C. A. Jones, J. Fluid Mech. **758**, 407 (2014).
- [26] B. Favier, C. Guervilly, and E. Knobloch, J. Fluid Mech. **864**, R1 (2019).
- [27] A. J. Aguirre Guzmán, M. Madonia, J. S. Cheng, R. Ostilla-Mónico, H. J. H. Clercx, and R. P. J. Kunnen, Phys. Rev. Lett. **125**, 214501 (2020).
- [28] K. Julien, A. M. Rubio, I. Grooms, and E. Knobloch, Geophys. Astrophys. Fluid Dyn. **106**, 392 (2012).
- [29] S. Maffei, M. J. Krouss, K. Julien, and M. A. Calkins, J. Fluid Mech. **913**, A18 (2021).
- [30] A. M. Rubio, K. Julien, E. Knobloch, and J. B. Weiss, Phys. Rev. Lett. **112**, 144501 (2014).
- [31] S. G. Huisman, R. C. A. van der Veen, C. Sun, and D. Lohse, Nature Communications **5**, 1 (2014).
- [32] C. Guervilly and D. W. Hughes, Physical Review Fluids **2**, 113503 (2017).
- [33] K. Julien, E. Knobloch, and M. Plumley, Journal of Fluid Mechanics **837**, R4 (2018).
- [34] M. Matsumoto, S. Saito, and I. Ohmine, Nature **416**, 409 (2002).
- [35] H. Watanabe, M. Suzuki, and N. Ito, Phys. Rev. E **82**, 051604 (2010).
- [36] R. F. Garmann, A. M. Goldfain, and V. N. Manoharan, Proc. Natl. Acad. Sci. **116**, 22485 (2019).
- [37] P. J. Metaxas, V. W. S. Lim, C. Booth, J. Zhen, P. L. Stanwix, M. L. Johns, Z. M. Aman, G. Haandrikman, D. Crosby, and E. F. May, Fuel **252**, 448 (2019).
- [38] M. Volmer and A. Z. Weber, Z. Phys. Chem. **119**, 277 (1926).
- [39] R. Becker and W. Döring, Ann. Phys. **416**, 719 (1935).
- [40] J. B. Zeldovich, J. Exp. Theor. Phys. **12**, 525 (1942).
- [41] A. van Kan, T. Nemoto, and A. Alexakis, Journal of Fluid Mechanics **878**, 356 (2019).
- [42] K. Binder, Reports on Progress in Physics **50**, 783 (1987).
- [43] G. Dar, M. K. Verma, and V. Eswaran, Physica D **157**, 207 (2001).
- [44] A. Alexakis, P. D. Mininni, and A. Pouquet, Phys. Rev. E **72**, 046301 (2005).
- [45] P. D. Mininni, A. Alexakis, and A. Pouquet, Phys. Rev. E **72**, 046302 (2005).
- [46] P. D. Mininni, A. Alexakis, and A. Pouquet, Phys. Fluids **21**, 015108 (2009).
- [47] M. K. Verma, A. Kumar, and A. Pandey, New J. Phys. **19**, 025012 (2017).
- [48] M. K. Verma, *Energy Transfers in Fluid Flows: Multiscale and Spectral Perspectives* (Cambridge University Press, 2019).